Egypt. J. Chem. **Vol. 64,** No. 7 pp. 3801 - 3816 (2021)

Egyptian Journal of Chemistry

http://ejchem.journals.ekb.eg/

Seawater Reinforces Synthesis of Mesoporous and Microporous Zeolites from Egyptian Fly Ash for Removal Ions of Cadmium, Iron, Nickel, and Lead from Artificially Contaminated Water

Lubna A. Ibrahim[1,2] and ElSayed ElBastamy ElSayed[2]

[1] *Water Management Research Institute (WMRI), National Water Research Center (NWRC), Qalyobia, 13621, Egypt.*

2 Central Laboratory for Environmental Quality Monitoring (CLEQM), NWRC, Qalyobia, 13621, Egypt.

Abstract

This study focuses on the production of mesoporous and microporous zeolites via fusion pre-treating fly ash with NaOH followed by hydrothermal treatment utilizing seawater. Three pretreatments for fly ash were carried out utilizing 1:1, 1.2:1, and 1.4:1 of NaOH:fly ash ratio to compare the removal efficiency for cadmium Cd(II), iron Fe(II), nickel Ni(II), and lead Pb(II) from artificially contaminated water. The impacts of several variables including concentrations, weights, pH, and contact times were examined to acquire knowledge on the adsorption rate. X-Ray Diffraction (XRD), Scanning Electron Microscope (SEM), and Brunaauer-Emmett-Teller (BET) were utilized to investigate zeolite structures. N_2 adsorption/desorption isotherms demonstrated that the synthetic zeolites were mesoporous and microporous materials with a higher specific area (347, 240, and 127 m^2/g) than the values for raw fly ash (15m^2/g). The X-ray diffraction outcome suggested that the synthetic products mainly belonged to phillipsite, carbonate cancrinite, and hydroxysodalite. These outcomes showed that fly ash and seawater from power plants are appropriate for synthesizing high-quality zeolites. For contaminated water treatment, the products are effective for removal Cd(II), Fe(II), Ni(II), and Pb(II) at pH 7, contact time 45 min, and dose 1 g/L. Zeolites recycling outcomes showed that the removal efficiency of investigated metal ions by Z1, Z2, and Z3 was reduced by an average of 7%, 5%, and 3% after regeneration.

Keywords: Adsorption; Fly ash; hydrothermal process; mesoporous zeolite; microporous zeolite.

1. Introduction

Water is an indispensable resource as God made from water each living thing. The genuine contamination of water is one of the critical reasons prompting the deficiency of water resources. Therefore, accelerating the legitimate use of water resources and a reasonable portion of sewage resources are significant approaches to lighten the deficiency of water resources. There are numerous strategies for the removal of metal ions as, Cd(II), Fe(II), Ni(II), Sr(II), Cs(I), and Pb (II) from wastewater [1-5]. However, the greater part of the remediation approaches includes complex methodology, equipment, and significant expense for wastewater treatment. Among them, adsorption has been affirmed to be a low-price innovation with high proficiency. Subsequently, the advancement of low-value adsorbents is the way to conquer the significant cost of removing heavy metals.

Fortunately, fly ash (FA) is a by-product of thermal power plants produced in an immense quantity yearly [1,6, 7]. Every year, the amount of FA generated worldwide was about 750 million tons [8], of which more than twenty-five million tons in South Africa [9], and over a hundred and seventy (70) million tons in urban areas of China. In particular, FA is a heterogeneous compound characterized by three constituents that are minerals (quartz, mullite, lime, hematite, and magnetite), unburned coal particles, and prevalent amorphous aluminosilicate phase [6, 7, 10]. Fly ash is utilized for a wide of applications as a soil

*Corresponding author e-mail: lubna736@hotmail.com & lubnaibrahim43@gmail.com; (Lubna A. Ibrahim).
Receive Date: 26 April 2021, Revise Date: 05 June 2021, Accept Date: 13 June 2021
DOI: 10.21608/EJCHEM.2021.73834.3661

stabilizer in a geotechnical application [11-15], construction material as an extender and pozzolan [16], and synthesis of zeolite for wastewater treatment [17].

The similarity of composition between fly ash and zeolite, which is mainly SiO_2-Al_2O_3-CaO-Fe_2O_3, makes it is possible to convert that ash to zeolite. Distinctive approaches have been utilized, the hydrothermal method by using an alkaline medium and with fusion pre-treatment at high temperatures for zeolite synthesis [18-25]. The distinctions concern solution/fly ash activation ratio, sort of solution, type and molarity of the alkaline agents, temperature, reaction time, pressure, and crystallization time. The use of seawater for zeolite synthesis is described in previous studies by Belviso [26] and Yanqing [27] at different temperatures and salinities.

It is significant that all kinds of zeolites, whether natural or industrial, are imported from outside Egypt. So, the problem can be summarized that there is no sufficient study on the recycling of Egyptian fly ash for the production of zeolite. In addition, water shortage or scarcity is one of the major worldwide issues of this century. So, it is imperative to look for non-conventional sources of water to reduce the gap between water supply and demand.

Therefore, this study aims to reuse Egyptian fly ash and high-temperature seawater produced from the cooling of the turbine in the thermal power plant in the production of zeolite, which has many uses, including treating contaminated water. The objectives of this article were to investigate the impact of using different NaOH/FA ratios on the reaction that occurs during the synthesis of zeolites was investigated. The synthetic zeolite products were characterized and depicted by X-Ray Diffraction (XRD), Scanning Electron Microscope (SEM), and Brunaauer-Emmett-Teller (BET) instruments. The synthesized products were applied on artificially contaminated water to investigate the effectiveness of removal of Cd(II), Fe(II), Ni(II), and Pb(II) ions at different concentrations, weights, pH, and times of contact. Finally, recovery experiments for the spent products were done.

2. Materials and methods

2.1. Reagents

Sodium hydroxide (NaOH), potassium chloride (KCl), HCl (36.0–38.0%), and HNO_3 (65%) were purchased from Sinopharm Chemical Reagent Co., Ltd. Stock single standard solutions 1000 mg/L of aluminium Al(III), barium Ba(II), cadmium Cd(II), chromium Cr(III), copper Cu(II), iron Fe(II), manganese Mn(II), lead Pb(II), nickel Ni(II), and zinc Zn(II) of guaranteed grade pure were purchased from Merck (Merck, Darmstadt, Germany). In the laboratory, deionized water and analytical chemical-grade were utilized for preparing all solutions. All plastic bottles were rinsed in 10% HNO_3 solution, and then rinsed with deionized water.

2.2. Fly ash collection

Egyptian fly ash was collected from Construction Research Institute (CRI), National Water Research Center (NWRC), Egypt.

2.3. Fly ash characteristics

A Pipette method was utilized for the identification of fly ash texture [29]. An extract with a ratio of 1 fly ash:5 water was left for 30 min for equilibration and then the extract was used for the determination of pH and EC. The oxidation method was utilized for organic matter (OM) determination [30]. Al_2O_3%, SiO_2%, CaO, Na_2O, TiO_2, MgO, and K_2O were estimated according to the American Society for Testing Material standard [30].

2.4. Laboratory analyses of water samples and Seawater characteristics:

The seawater utilized in this investigation was gathered from the outlet of the Suez power plant and collected in a polyethylene bottle. The contaminated, treated water and seawater were preserved and analyzed relying on standard methods [28]. For major cations and heavy metals, the samples filtered by the filtration system through a membrane filter of pore size 0.45 µ and acidified with nitric acid to pH <2, to prevent any change in the chemical composition of the sample before the examination, and the other two bottles were free from any added substance.

Major cations (calcium (Ca^{2+}), potassium (K^{+}), magnesium (Mg^{2+}), and sodium (Na^{+}), chloride (Cl^{-}), sulphate (SO_4^{2-}), were analyzed by ICS-1100 ion chromatography (Thermo Scientific, USA).

Heavy metals (Al^{2+}, Ba^{2+}, Cd^{2+}, Cr^{3+}, Cu^{2+}, Fe^{2+}, Mn^{2+}, Pb^{2+}, Ni^{2+}, and Zn^{2+}) were predestined in water by utilizing Inductively Coupled Plasma-Optical Emission Spectrometry (ICP-OES) Dual View. Recovery for the heavy metals determined by ICP-OES ranged between 95 and 102%.

2.5. Synthesis of zeolite

Fusion technique joined with hydrothermal treatment was performed for the zeolite synthesis relying on a modification Molina and Poole [21] method. In particular, 4 g fly ash was blended with various (1:1,

1.2:1, and 1.4:1) NaOH/fly ash ratios to get a homogeneous mixture for Z1, Z2, and Z3, respectively. After that, it was heated in a crucible at 550 ◦C for 2 h. The fusion products were cooled then ground and dissolved in 45 mL seawater, and the mixtures were transferred into 100 mL reaction bombs followed by an aging process with vigorous shaking at room temperature for 12 hours. The mixtures were then crystallized under static conditions at a steady temperature of 45 °C for 48 hours. The solids were regenerated by vacuum filtration, washed a few times with deionized water, and then dried overnight at 105 °C. This experiment was duplicated to contemplate study the process repeatability.

2.6. Characterization (XRD and SEM)

Zeolite Z1, Z2, and Z3 were identified utilizing X-Ray Diffraction (XRD), and scanning electron microscope (SEM). X-Ray Diffractometer (XRD, BrukerD8 Advance, Germany) was utilized to determine the crystalline phases of synthesized products, utilizing CuKα as a radiation source (45 KV, and 250 mA, and scanning rate of 2°/min from 10 to 70° was performed. A software Joint Committee of Powder Diffraction Standards (JCPDS) and data published by Treacy and Higgins [31] were utilized to identify the crystalline phases. Morphology characterization for Z1, Z2, and Z3 synthesized zeolites was done after drying and coating (gold–palladium) by utilizing the PHENOM ProX desktop scanning electron microscope (SEM, AM Eindhoven, The Netherlands).

2.7. Surface Area Measurements

The surface area analysis, pore-volume, and pore size of the prepared zeolites were estimated by Brunauer-Emmett-Teller (BET, HitachiVP-SEM S-3400N, Germany) method.

2.8. Adsorption experiments

The initial metal concentrations, product dosage, contact time, and pH were examined to properly choose the optimizing conditions of the adsorption process. Artificial wastewater containing ions of Cd(II), Fe(II), Ni(II), and Pb(II) is prepared in Central Laboratory for Environmental Quality Monitoring (CLEQM). Wastewater samples were collected from the outlet of Suez Bay Industrial Wastewater Treatment Plant at Ataqa Region [32] and spiked with standard solutions for cadmium, iron, nickel, and lead (1000 mg/L) to utilize in the adsorption experiment. The adsorption of Cd^{2+}, Fe^{2+}, Pb^{2+}, and Ni^{2+} by zeolite is investigated by discontinuous adsorption experiments, which were carried out thrice at a constant temperature of 25 °C and shaken at 120 rpm for 1 h.

- Impact of initial metal ion concentration: The impact of various concentrations (20, 40, 80, 100 mg/L) for solutions containing Cd^{2+}, Fe^{2+}, Pb^{2+}, and Ni^{2+} on the efficiency of removal was investigated at fixed zeolites products dose (0.1 g/0.1 L). The removal efficiency was calculated according to equation 1, where the initial (C_i) and final (C_f) concentrations of the studied parameters Cd(II), Fe(II), Ni(II), and Pb(II) [33].

$$Removal\ efficiency\ \ (\%) = \left[\frac{(Ci - Cf)}{Ci}\right] \times 100 \qquad (1)$$

- Impact of dosage: The removal efficiency of synthesized zeolite products was examined by studying the application of different weights from the products (0.05 g, 0.1 g, 0.2 g, 0.4 g, and 0.8 g) on 0.1 L solution containing a concentration of 50 mg/L. The adsorption capacity (q_e) of the adsorbent zeolites Z1, Z2, and Z3, q_e (mg metal / g dry adsorbent) can be calculated from equation 2, where V (L) is the volume of solution and W (g) is the amount of dry adsorbent [24].

$$q_e = (Ci - Cf)\frac{V}{W} \qquad (2)$$

- Impact of Contact time: The investigation did with a fixed product dose (0.1 g of prepared zeolites Z1, Z2, and Z3 / 0.1 L of 100 mg/L artificially prepared solution). All samples, in addition to the raw contaminated sample, were shaken for 15, 30, 45, and 60 min.
- Impact of pH: Study pH effect on zeolite Z1, Z2, and Z3. Fixed products dose (0.1 g/ 0.1 mL) were utilized in various pH; 4, 7, 8, and 20, of artificially contaminated wastewater by 10 mg/L Cd(II), Fe(II), Ni(II), and Pb(II) were researched. 0.01M HCl and 0.01M NaOH solutions were utilized to modify the pH values of the contaminated water samples.

2.9. Regeneration of zeolites

Successive adsorption/desorption investigation was done (5 trials). Recycling of zeolites was carried out by chemical treatment; in which zeolites were washed gently with 1 M KCl, to remove the desorbing metal ions from its surface, then rinsed with deionized water to eliminate any leftover KCl and then dried at 80 °C [34]. In final, the recycled and originally synthesized zeolites

were exposed to artificially contaminated water by 100 mg/L Cd (II), Pb(II), Fe(II), and Ni(II) for performance evaluation. *2.10. Statistical analysis*

The analyses were done thrice for all experiment. SPSS, ver. 15, 2006, statistical model was utilized to estimate the mean values and relative standard deviation (RSD) through this study.

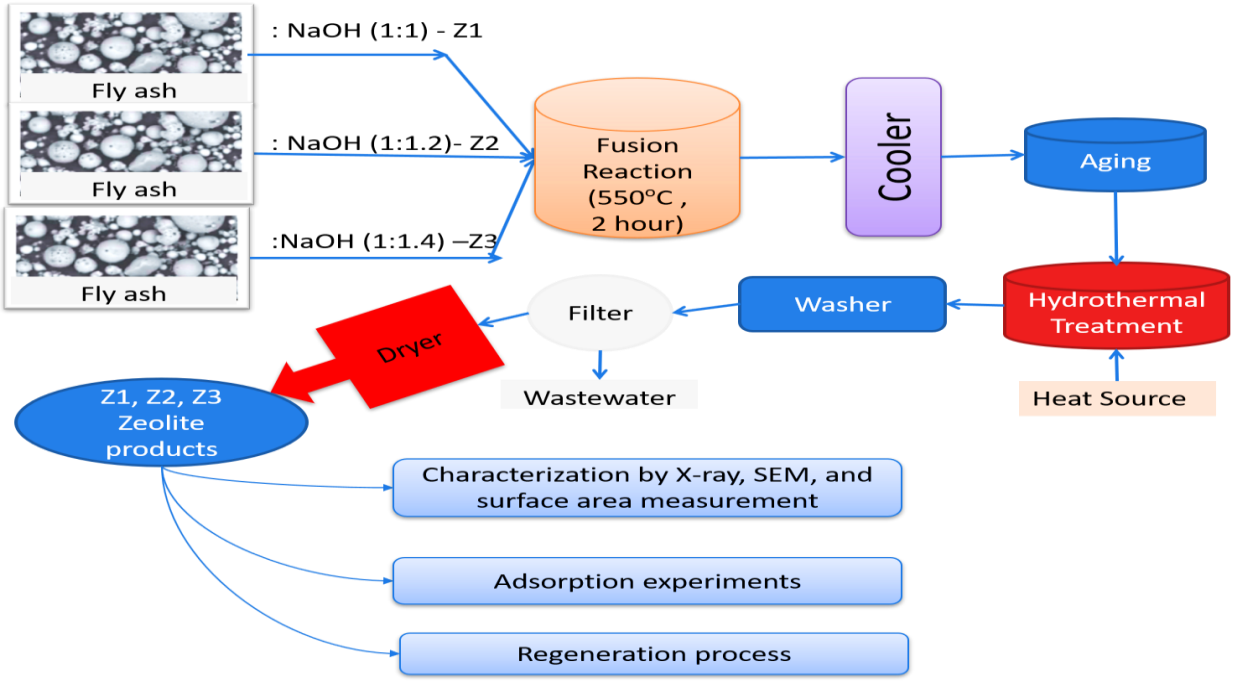

Fig. 1. Sketch diagram showing the methodology of preparation of mesoporous zeolite products Z1, Z2, and Z3

3.Result and discussion

3.1. Characteristics of fly ash and seawater

Fly ash utilized in this investigation has a dark gray color; this color is commonly ascribed to elevated unburned carbon content. The data indicated that fly ash was alkaline, with pH 10.28 ± 0.01. Organic matter content was 1.37±0.006 %. The result of texture analysis showed that fly ash samples comprise fine sand (26.44%±0.03), clay (16.30%±0.02), and silt (57.26%±0.03) indicating that fly ash was silt loam texture [35].

The particles are generally spherical in size 10 µm as shown in Fig. (2). The results indicated that the untreated raw fly ash particles are cenospheres hollow spherical with a relatively smooth surface texture. The physical properties and chemical compositions of the raw fly ash utilized in the zeolite preparation appeared in Table 1 and Fig. 3, respectively. The SiO_2/Al_2O_3 ratio of the ash is approximately 2.02, demonstrating that this type of ash is favorable for use as a raw material for low Si zeolite synthesis [36]. Moreover, the fly ash also has lower Fe and Ca content (4.9% Fe_2O_3 and 3.41% CaO). The presence of Fe indicates the presence of magnetite which acts as inert material for zeolite synthesis but calcium acts as an inhibitor in the case of the formation of calcium silicate.

The chemical compositions of seawater used in the preparation of fly ash are outlined in Table 2. The average values for TDS, EC, calcium, potassium, magnesium, and sodium are 60.39 mS/Cm, 42280 mg/L, 394 mg/L, 135 mg/L, 3785 mg/L and 27333 mg/L, respectively. The abundant Na^+ cations in the seawater act as a trigger for the ordered arrangement of the zeolite structure [27]. The cations in the solution play an important role in attacking the silicon and

aluminium contained in the starting material and in balancing the zeolite structure [27]

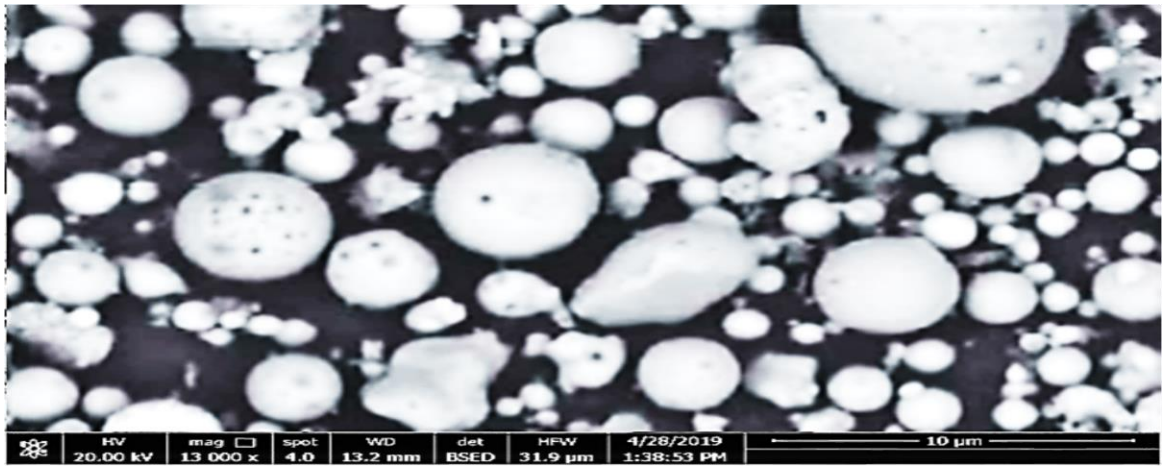

.**Fig. 2.** SEM image for raw fly ash (10 µm, 13000x).

Table 1
The physical variables of the raw fly used for zeolites synthesis.

Metal oxide	Amount (wt%±SD)	Metal oxide	Amount (wt%±SD)
pH (dimensionless)	10.28	fine sand	26.44±0.03
Organic matter	1.37±0.006	clay	16.30±0.02
LOI	0.85±0.04	silt	57.26±0.03

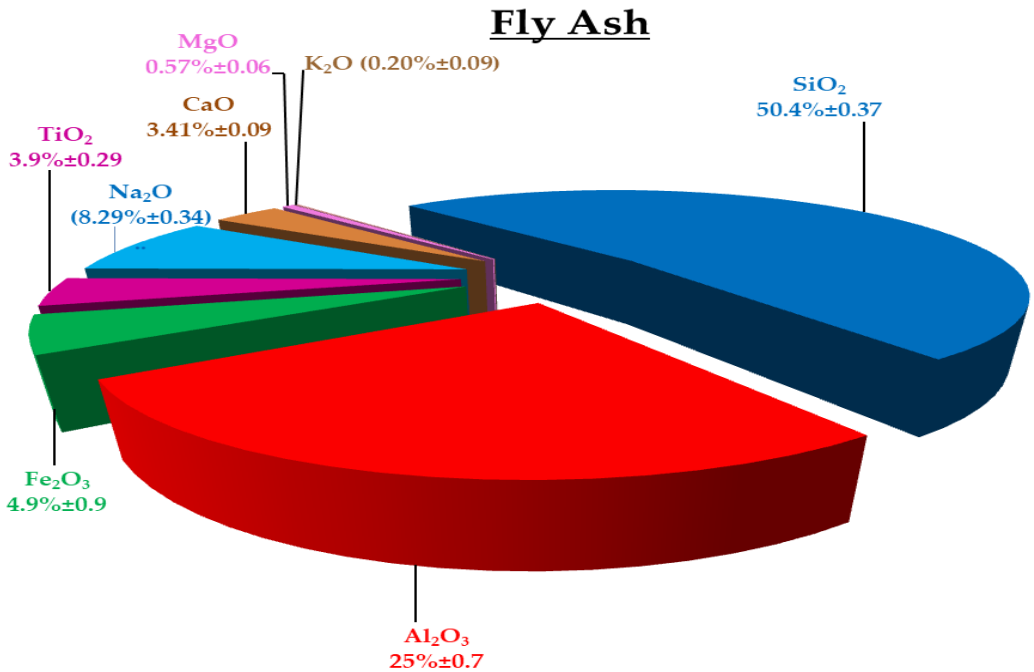

Fig. 3. Chemical composition (mean±SD) of the raw fly ash utilized in zeolites synthesis.

Table 2
Physical and chemical parameters of seawater used for zeolites synthesis.

Parameters	Concentration (mg/L)	Parameters	Concentration (mg/L)
pH (dimensionless)	7.4	Sulfate	2070
Alkalinity	142	Aluminum	0.012
EC	60.39 (mS/cm)	Barium	0.031
Calcium	912	Chromium	0.005
Magnesium	236	Copper	0.041
Potassium	131	Iron	1.34
Sodium	12510	Manganese	0.21
Chloride	19214	Zinc	0.01
Sulfate	2070	Cadmium	0.002

The mechanism of the zeolite formation process in our study includes three stages of zeolite formation which are the primary amorphous phase, nucleation or secondary amorphous phase, and zeolite crystal growth [37]. The reaction between NaOH and the principal component of fly ash (mullite and quartz) results in the formation of silicate and aluminate via damaging the crystal structure, reactions 1 & 2. The formation of aluminate and silicate doesn't happen when utilizing a small amount of NaOH, while a higher amount of NaOH caused micro-cracks on the particle [38]. Most of the Si and Al components remain in the amorphous aluminosilicate phase because the dominant crystal growth of zeolite prohibits zeolite nucleation. Also, NaOH reacts with silicon and aluminium in a subsequent hydrothermal reaction which in turn enhances the precipitation of geopolymers (gel) [38, 39].

In the final stages of synthesis, the secondary amorphous phase is converted into crystalline zeolite because of the progressive and continuous chemical reaction between the eluted ions (seawater) and the surface of the amorphous aluminosilicate phase. The chemical reactions 1,2, & 3 are as follows [19, 39]:

$$2\,NaOH + SiO_2 \xrightarrow{fusion} Na_2SiO_3 + H_2O \quad \textbf{(1)}$$

$$10NaOH + 3Al_2O_3.2SiO_2 \xrightarrow{fusion} 2Na_2SiO_3 + 6NaAlO_2 + 5H_2O \quad \textbf{(2)}$$

$$NaOH(aq) + Na[Al(OH)_4](aq) + Na_2SiO_3 \rightarrow [Na_x(AlO_2)_y.NaOH.H_2O]\,(gel) \rightarrow Na_p(AlO_2)_p.(SiO_2)_q.hH_2O\,(crystal) \quad \textbf{(3)}$$

This chemical reaction is mediated by Na^+ cations in the homogeneous solution. The abundant Na^+ cations in the seawater act as a trigger for the arrangement of the zeolite structure. The cations in the solution play an important role in attacking the silicon and aluminum contained in the starting material and in balancing the zeolite structure.

3.2. Characteristics of the synthesized products

The synthesized zeolite Z1, Z2, and Z3 were portrayed by XRD and SEM. The XRD pattern for zeolites Z1, Z2, and Z3, which have been synthesized at different dosages of NaOH/ash ratios = 1, 1.2, and 1.4, respectively, are represented in Fig. 4. The data of our investigation was compared with the data reported in the literature by Treacy and Higgins [31]. In Fig. 4, the presence of diffraction peaks at 2Θ=29.4 °, which decrease in the order of Z2› Z1 = Z3 revealed the presence of $CaCO_3$.
For Z1, the XRD peak appeared at 2Θ= 11.69 ° refers to Na-X but the peak at 21.67° refers to Na-P1 [31]. The primary peaks appeared at 2Θ= 12.36°, 27.8 °, 30.3 °, 32.5°, 34.7°, 35.6 °, 40.51°, 41.95°, 43.37°, and 45.29°, angle degree confirmed the presence of phillipsite mineral $[K_2Ca_{1.7}Na_{0.4}(H_2O)_{13.5}][Si_{10.6}Al_{5.3}O_{32}]$ [31]. The small zigzag peaks that appeared in Fig. 4 refer to the presence of amorphous material, while the strong peaks represent full crystallization. The result verified the transformation of zeolite X to a more stable phillipsite mineral in the monoclinic phase [40] as a result of Zeolite Na-P1 of increment co-solvent ratio. Therefore, the outcomes showed that using NaOH as activators to fly ash with a 1:1 ratio for synthesizing zeolite indicated that mainly zeolite phillipsite, Na-P1, and Na-X have been synthesized similar to the findings of Querol et al. [41].

XRD pattern of the sample Z2 is identified by primary peaks at 2Θ= 15.3°, 26.84°, 27.4°, 30.08 °, 32.8°, 33.4°,

35.7°, 36.92°, 39.76°, 42.7°, indicating the appearance of carbonate cancrinite [Na_6Ca_2 $Si_6Al_6O_{24}$ $(CO_3)_{2..}2(H_2O)$] according to Treacy and Higgins[31] and JCPDS (A software Joint Committee of Powder Diffraction Standards) No. pdf # 1-71-776 [42]. Concerning the calcium oxide (CaO) recognized in the starting material (raw fly ash) which probably gave rise to calcite ($CaCO_3$) during the oven drying process. The presence of XRD reflections appointed to cancrinite demonstrated the crystallization of Al and Si species and reaction with $CaCO_3$ (present in the fly ash) to form carbonate cancrinite, Reaction 4 [42]. Sodalite was identified by distinctive reflection at, 14.02°, 24.4°, 32°, and 49.8° (2Θ) degrees. This preferential crystal growth of sodalite in seawater may be attributed to the lower activation energy required for nucleation. While the small peaks indicate the presence of calcium silicate hydroxide ($Ca_{4.5}Si_6O_{15}(OH)_3{\cdot}2H_2O$).

$$3Al_2O_3.2SiO_2.H_2O + CaCO_3 + 6NaOH \rightarrow Na_6Al_6Si_6O_{24}(CaCO_3)2H_2O + 4H_2O \quad \textbf{(4)}$$

The XRD primary peaks of Z3 mineral appeared at diffraction peaks centered at 2Θ=14°, and 24.5° angle degree refer to hydroxysodalite [$Na_8Al_6Si_6O_{24}(OH)_2(H_2O)_2$] according to Treacy and Higgins[31] and JCPDS No. pdf # 1-72-2329 [42]. While the primary peaks appear at 2Θ = 21.7°, 27.34°, 32.85°, 35.32°, 40.08 °, 41.6°, 42.85°, 44.75°, and 45.7° demonstrated the appearance of cancrinite [$Na_7Ca_{0.9}(CO_3)_{1.4}(H_2O)_{2.1}$][$Si_6Al_6O_{24}$] according to Treacy and Higgins [31] and JCPDS No. pdf # 1-71-776) [42]. The presence of XRD reflections assigned to cancrinite and hydroxy-sodalite results from the consumption of carbonate and the hydroxy-sodalite started to crystallize, Reaction 5 [42].

$$3Al_2O_3.2SiO_2.H_2O + 8NaOH \rightarrow Na_8Al_6Si_6O_{24}OH_2 + 2H_2O \quad \textbf{(5)}$$

It was observed that the increase in sodium hydroxide in the synthesis reaction was determinant in the formation of a new phase, the cancrinite, due to the higher alkalinity of the medium, which facilitated the dissolution of both the initially formed zeolitic phase, the sodalite, and the other compounds present in the sample so that the elements were available for this phase transformation. Probably, when submitted to 36 h of treatment, a reversible reaction occurred that caused the dissolution of the cancrinite phase. Similar findings by Reyes [43], had also obtained similar results in which sodalite was transformed and cancrinite zeolite. Where the authors stated that a longer reaction time promotes a more efficient dissolution of the starting materials, and characterized by an increase in the intensity ratio of the sodalite and cancrinite XRD peaks. The authors also affirmed that there is difficulty in distinguishing the peaks and quantifying the phases of sodalite and cancrinite because in XRD analysis there is an overlap of these peaks due to structural similarity. The cancrinite phase is formed through the dissolution of sodalite and subsequent precipitation in the form of cancrinite zeolite, considered to be chemically more stable than sodalite [20].

Finally, Fig. 4 indicates that the ratio NaOH/ash 1:1.4 shows better crystallization of the zeolite followed by 1:2, and 1:1.1.

The surface area of fly ash and the synthesized Z1, Z2, and Z3 samples were depicted by N_2 adsorption/desorption isotherms (BET), Fig. 5. The nitrogen adsorption-desorption isotherms of the synthesized zeolites Z1, Z2, and Z3 are identified as type IV following the International Union of Pure and Applied Chemistry (IUPAC) classification, Fig. 5. This type of physisorption isotherm is characteristic of mesoporous (2–50 nm) adsorbents for Z1 and microporous (less than 2 nm) for Z2, and Z3 [44], which is favorable for the ion exchange process because it affords more access sites for sorbate cations to approach the inner mesoporous and micropores within the zeolite structure [45]. As seen from Table 3, the most crystalline material Z3 has a micropore volume of 0.282 cm^3/g followed by Z2 material (0.183 cm^3/g) and Z3 (0.140 cm^3/g).

As displayed in table 3, fly ash has a 15 m^2/g specific BET surface area. Whereas, the measured specific surface area for zeolite Z1, Z2, and Z3 was found to be 127.56 m^2/g, 346 m^2/g, and 127.56 m^2/g, and the average particle radius was seen to be 1.52 nm, 1.62 nm, and 2.21 nm, respectively. The treatment of fly ash by NaOH increases the surface area of the particle by up to 8, 16, 23 times that of the raw fly ash. The high BET surface area for the synthesized zeolites Z3 > Z2 > Z1 is preferable for providing large adsorption capacity, so it means that zeolite may be used as an adsorbent of many pollutants like heavy metals, radionuclides, etc.

Recognizing the role of the surface on catalytic activity, the surface morphology of the synthesized zeolite was evaluated using SEM. The SEM images of the samples Z1, Z2, and Z3 (NaOH/ash ratios = 1, 1.2, and 1.4, respectively) indicate the existence of the sample as a porous material, which is one of the important characteristics of a heterogeneous catalyst. In comparison to Fig. 2., the absence of the spherical particles indicates the high conversion of fly ash to crystalline zeolite on the hydrothermal method. The crystal structure of the synthesized zeolite was with different particle sizes and morphology, which can be

attributed to the difference in the preparation of synthesis solution NaOH/ash ratios. After consuming NaOH the rest fly ash retained the initial spherical morphology of the fly ash, but the sphere surface became much rougher.

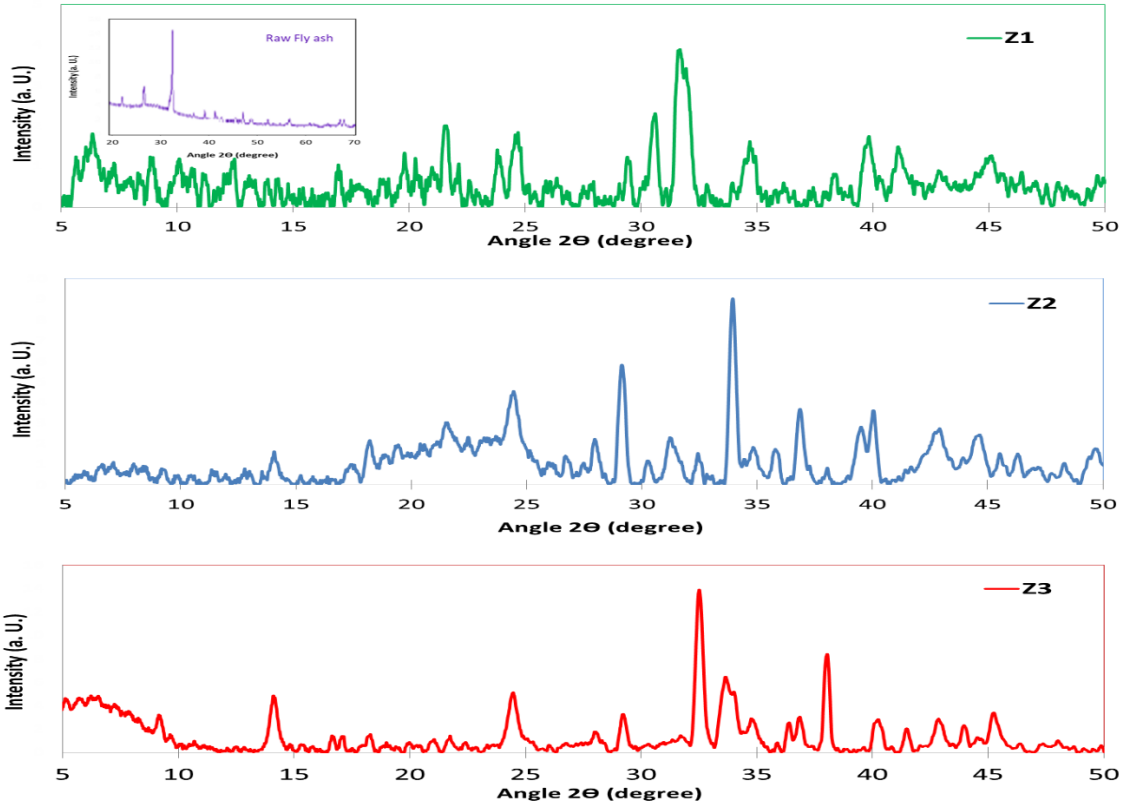

Fig. 4. X-ray diffraction spectroscopy (XRD) pattern of the synthesized zeolite samples Z1, Z2 and Z3 prepared with NaOH/ash ratios = 1, 1.2 and 1.4, respectively.

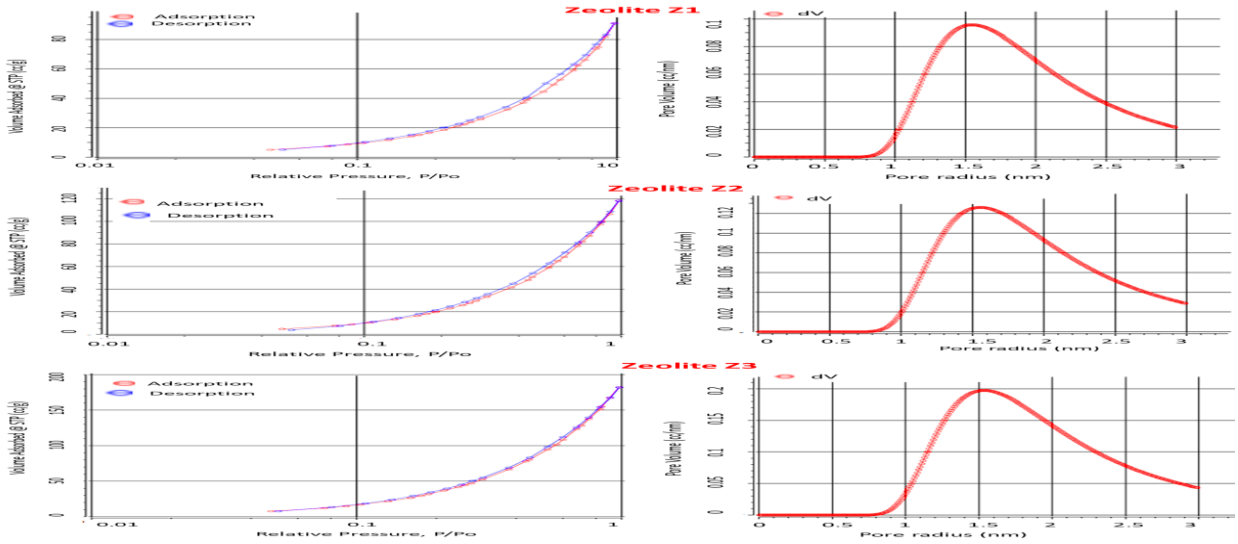

Fig. 5. N2 sorption isotherms for the hydrothermal alkali-activation products of Egyptian fly ash prepared with NaOH/ash ratios = 1, 1.2 and 1.4, for Z1, Z2, and Z3, respectively.

Table 3
Brunauer–Emmett–Teller (BET) analysis for raw fly ash and synthesized zeolite products using different ratios of NaOH/ash.

	BET Surface area	Average particle size	Total pore volume
Raw fly ash	15 m^2/g	-	-
Z 1	127.569 m^2/g	2.21005 nm	0.140967 cc/g (cm^3/g)
Z2	240.607 m^2/g	1.52396 nm	0.183337 cc/g (cm^3/g)
Z3	346.592 m^2/g	1.62892 nm	0.282285 cc/g (cm^3/g)

Z1, Z2, and Z3 are the synthesized zeolite at NaOH/ash ratios = 1, 1.2, and 1.4, respectively.

Fig. 6 represents the morphology of Z1 at different magnifications. The images (A & B) produced at low magnification (200 x and 800x) indicated the presence of clusters of different sizes and shapes as a result of particle agglomeration. Further, increased magnification to 6000 x (C) illustrated that the two different shapes of the grains can be distinguished, i.e. distorted octahedral, and cubic crystals. These crystal shapes are more evidently displayed by the image obtained at the highest magnification (12000x and 24000x) which demonstrated distorted octahedral crystals (growth of crystals parallel in three dimensions) for zeolite Na-x, fibrous of Na-P1, and cubic crystals from phillipsite arranged into elongated stubby laths. In the same manner, different crystal shape of zeolite-X crystal was reported by [46]. In this respect, different crystal shapes of zeolite-X are probably associated with Na-P1 and phillipsite.

Fig. 7 for Z2, the image produced at low magnification (1000 x) indicated the presence of clusters, while the magnification to 2000x, 4000x, 7000x and 13 000x produced an image with three different shapes of the grains. The highest magnification at 25 000x illustrated three crystals which are pseudohexagonal of hydroxysodalite zeolite, crystals with noodle-like of cancrinite, and amorphous species of calcium silicate. According to [47], cancrinite formed as more tiny hexagonal needles in the lepispheres.

Fig. 8 represents the morphology of Z3 at different magnifications. The image produced at low magnification (200x, 800x, 3000x, and 6000x,) indicated the presence of clusters of different grains with different sizes and shapes. The highest magnification (12000x and 24000x) indicated crystals with noodle-like cancrinite, and elongated rhombohedra crystals of hydroxysodalite are present.

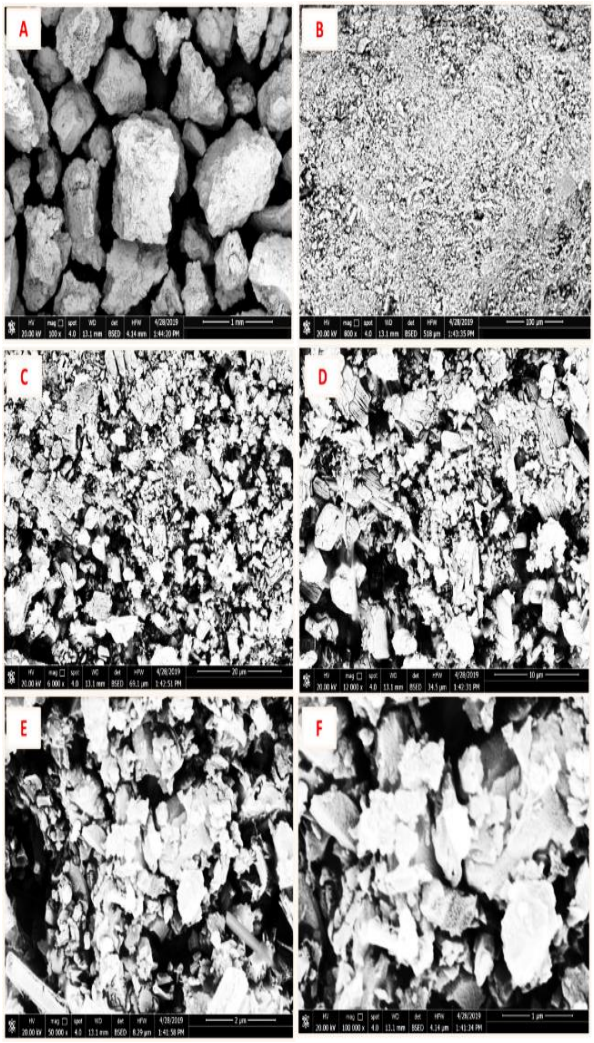

Fig. 6. SEM images of zeolite Z1 (NaOH/ash ratios = 1.4) with different magnifications (A) 100 x; (B) 200 x; (C) 6000 x; (D) 12 000 x; (E) 50 000 x, and (F) 100 000 x.

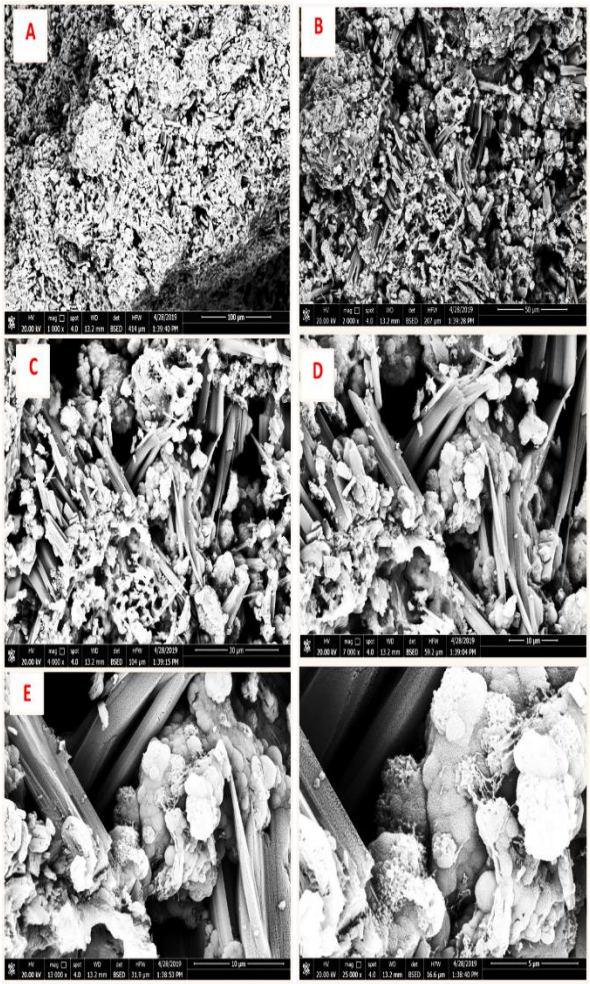

Fig. 7. SEM images of zeolite Z2 (NaOH/ash ratios = 1.2) with different magnifications (A) 100 μm, 1000 x; (B) 50 μm, 2000 x; (C) 30 μm, 4000 x, (D) 10 μm, 7 000 x; ((D) 10 μm, 13 000 x;. and (E) 5 μm, 25 000 x.

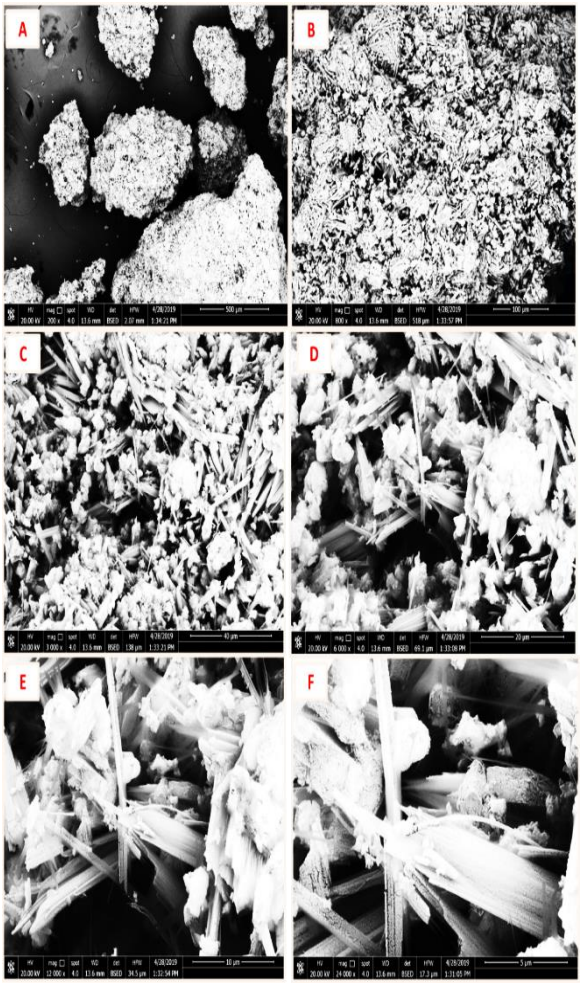

Fig. 8. SEM images of zeolite Z3 (NaOH/ash ratios = 1.4) with different magnifications (A) 200 x; (B) 800 x; (C) 3000 x; (D) 6000 x; (E) 12000 x, and (F) 24000 x.

3.3. Adsorption Studies

The take-up of heavy metals on synthesized zeolites has been widely examined [45]. Most investigations considered it as a cation exchange process amongst metal cations present in water and cations in the zeolite shape [45]. The scientific community also proposed the adsorption of metal ions results from the surface reaction amongst metal cation and hydroxyl groups on the zeolite framework [45]. The reaction can be represented in the next equations (6-9). Whereas equations (6-8) address the surface reaction and charge combination, and Equation 9 addresses the ion exchange mechanism. M'(z) is the metal cation (generally Na^+ or Ca^{2+}) in the zeolite structure. MOH^+ is the hydrolyzed divalent metal cation (M^{2+}) in the aqueous solution.

$$n\,Si-OH + M^{n+} \leftrightarrow (Si-O)_n - M + nH^+ \quad (6)$$

$$SiO^- + MOH^+ \leftrightarrow SiOMOH \quad (7)$$

$$nSiO^- + M^{n+} \leftrightarrow (Si-O)_n - M \quad (8)$$

$$nMOH^+ + M'(z) \leftrightarrow M_n(z) + M'^{n+} + nOH^- \quad (9)$$

Factors affecting the removal efficiency of elements from aqueous solution were examined to properly choosing the optimum parameter for simultaneous or synchronous adsorption process.

3.3.1. Effect of initial metal ion concentration on metal ion uptake by zeolite

Fig. 9 shows the efficiency of synthesized zeolite Z1, Z2, and Z3 as an adsorbent for Cd(II), Fe(II), Pb(II), and Ni(II) in simultaneous adsorption experiments for a concentration range of 20–100 mg/L. The outcomes of Fig. 8 demonstrated that the percent of removal increases as the concentration of metal ions Cd(II), Fe(II), Pb(II), and Ni(II) decreases. Whereas, the mechanism of metal ions uptake particularly relying on their initial concentration; at low concentrations, metal ions are adsorbed by specific active sites on zeolite Z1, Z2, and Z3 products, while with increasing metal ion concentrations the specific sites are somewhat saturated. For Z1, Z2, and Z3, the decline in the removal efficiency followed a trend of Pb(II)> Cd(II) > Ni(II)> Fe(II). This could be inversely proportional to the hydrated ionic radii as 4.01 Å for Pb(II) < 4.04 Å for Ni(II) < 4.26 Å for Cd(II), < 4.28 Å for Fe(II),). This means that the smaller the ionic radius, the more closely and strongly is the ion adsorbed [19, 45]. Because the smaller cations have more chance to pass through the micropores, mesopores, and channels of the synthetic zeolites [24, 48].

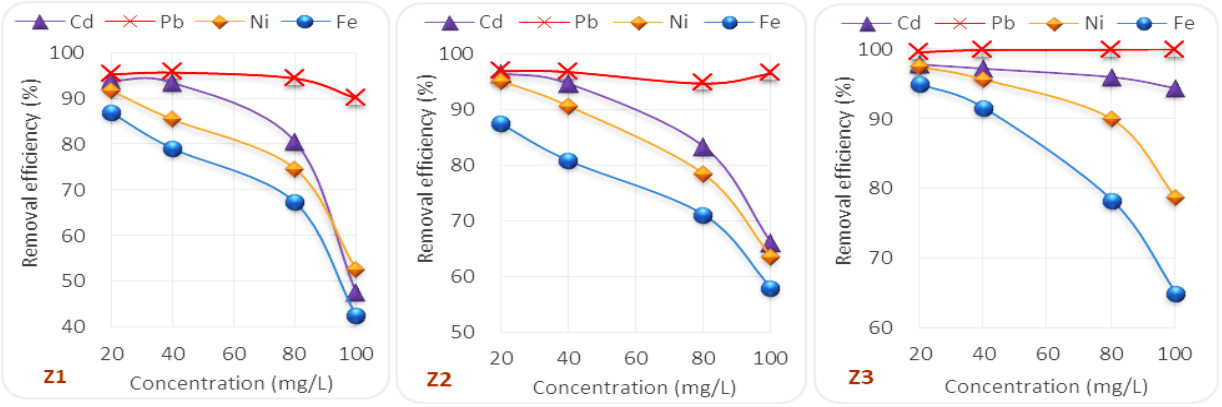

Fig. 9. Effect of initial metal ions on adsorption of (Cd(II), Fe(II), Pb(II), and Ni(II)) by zeolite products Z1, Z2, and Z3.

3.3.2. Impact of the initial weight of adsorbent zeolite products

In Figs. 9 and 10, the removal rate and adsorption capacity of Cd(II), Fe(II), Pb(II), and Ni(II) change with the amount of zeolite added. As illustrated by the adsorption curve, when the amount of zeolite increments from 0.5 g/L to 8 g/L, the removal rate of Cd(II), Fe(II), Pb(II), and Ni(II) increased linearly, Fig. 10. This is because with the increase of the amount of zeolite, adsorption sites increment, bringing about a fast increment in the removal rate of Cd(II), Fe(II), Pb(II), and Ni(II) [49]. However, the content of Cd(II), Fe(II), Pb(II), and Ni(II) in water is limited, with the increase of the amount of zeolite, an enormous number of abundance adsorption sites will definitely lead to adsorption capacity decline, Fig. 10. After that, the removal rate of Cd(II), Fe(II), Pb(II), and Ni(II) increment slowly with the increase of the quantity of zeolite. When the amount of zeolite increases to 1 g/L, the removal rate for Cd(II), Fe(II), Pb(II), and Ni(II) by for Z1, Z2, and Z3 stabilizes at less than 70-92, 83-95, and 86-95%, While the adsorption capacity is 35-46, 42-48, 43-48 mg/g, respectively, Fig. 11. Additionally, extreme crowding or grouping of zeolite particles causes interference on adsorption sites. Finally, in view of the thought of saving the amount of zeolite and ensuring the removal effect of Cd(II), Fe(II), Pb(II), and Ni(II), the amount of addition utilized in the following examination is 1 g/L with adsorption capacity 40 mg/g.

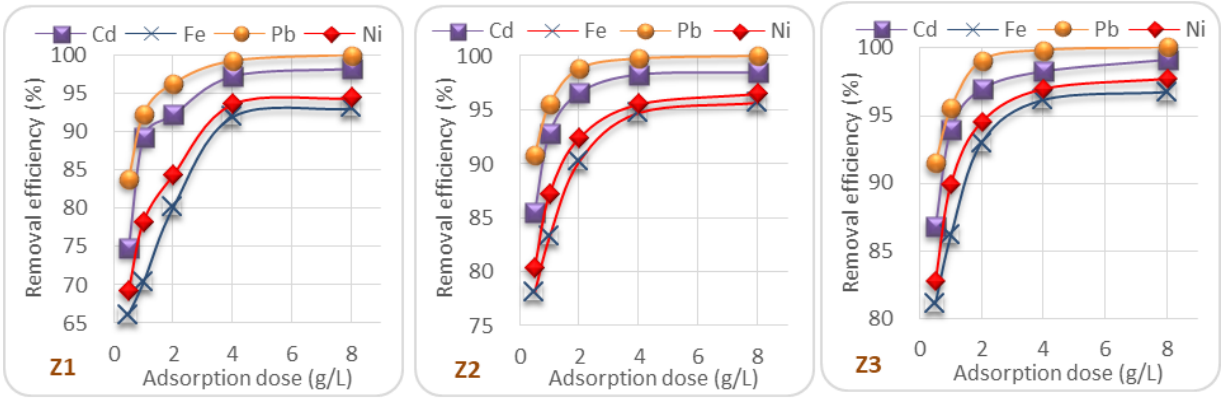

0

Fig. 10. Effect of zeolite addition (Z1, Z2, and Z3) on removal efficiency (%) of Cd(II), Fe(II), Pb(II), and Ni(II) from wastewater.

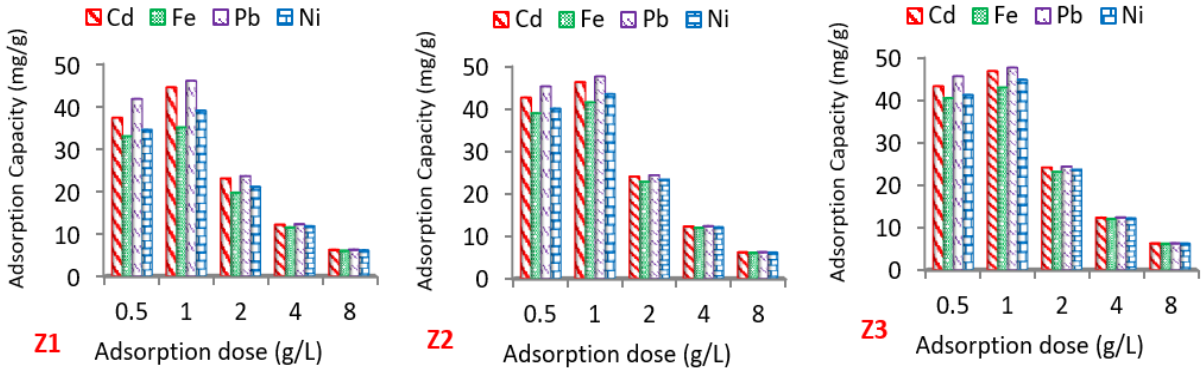

Fig. 11. Effect of zeolite addition on adsorption capacity (mg/g) of Cd(II), Fe(II), Pb(II), and Ni(II) by zeolite products Z1, Z2, and Z3.

3.3.3. Impact of contact time

The estimation of the ideal time is a significant variable in a wastewater treatment system. Overall for a given concentration, the amount of Cd(II), Fe(II), Pb(II), and Ni(II) ions adsorbed increments quickly with time in the beginning, then non-linearly reduce at a slower rate and finally attain saturation at equilibrium time, which is relying on concentration for every adsorbent ion, Fig. 12. For Z1, Z2, and Z3, at 15 to 30 min, the removal rate and adsorption capacity of Cd(II), Fe(II), Pb(II), and Ni(II) increased rapidly; however, at 30 to 45 min, the removal rate of Cd(II), Fe(II), Pb(II), and Ni(II) increment very slowly and reached equilibrium somewhere between 45 and 60 min. Finally, the ideal time for removal Cd(II), Fe(II), Pb(II), and Ni(II) by zeolite Z1, Z2, and Z3 is 45 min.

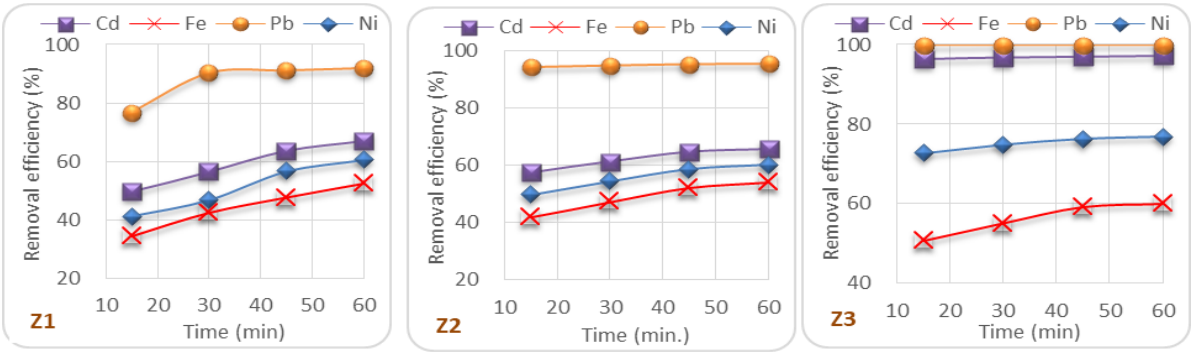

Fig. 12. Effect of contact time on adsorption of Cd(II), Fe(II), Pb(II), and Ni(II)) by zeolite products Z1, Z2, and Z3.

3.3.4. Impact of pH

One of the most principal parameters in the adsorption investigation that influence the adsorption behaviour of Cd(II), Fe(II), Ni(II), and Pb(II) in water is pH. Adsorption of different metal ions on the synthesized zeolite products Z1, Z2, and Z3 was studied at pH 4, 7, 8, and 10 values to optimize the maximum metal ion removal. The progressions of Cd(II), Fe(II), Pb(II), and Ni(II) removal rate with pH appear in Fig. 13. At the point when the pH of the solution is 4 the removal rates for Cd(II), Fe(II), Pb(II), and Ni(II) are 78, 63, 80, and 69% for Z1, but for Z2 are 79, 70, 84, and 78%, and 92, 82, 96, and 87% for Z3, respectively. Because at low pH, there is a large amount of H+ in the solution that preempts the adsorption site with Cd(II), Fe(II), Pb(II), and Ni(II) and forms competitive adsorption and for this, the rate of removal for these ions by Z1, Z2, and Z3 is low [45]. By increasing the pH to 7, the removal rate increments quickly, and reaches 90, 81, 99, and 94% for Z1, while 90, 83, 99, and 95% for Z2, and 98, 96, 99, and 97% for Z3, respectively. However, increasing pH from 7 to 8, and 8 to 10 the removal rates showed non-linearly slower rate and attained saturation. Because, when the pH value increments and the alkaline environment predominates, the hydroxide ion OH^- in the solution can easily react with Cd(II), Fe(II), Ni(II), and Pb (II) to form $Cd(OH)_2$, $Fe(OH)_3$, $Ni(OH)_2$, and $Pb(OH)_2$ precipitate, respectively [45]. At this time, not only the adsorption of synthetic zeolite to Cd(II), Fe(II), Pb(II), and Ni(II) but also the precipitation of hydroxide. Finally, to investigate the adsorption of synthetic zeolite to each of Cd(II), Fe(II), Pb(II), and Ni(II) and eliminate the impacts of competitive adsorption and precipitation, the pH of the examination solution was chosen as 7.0.

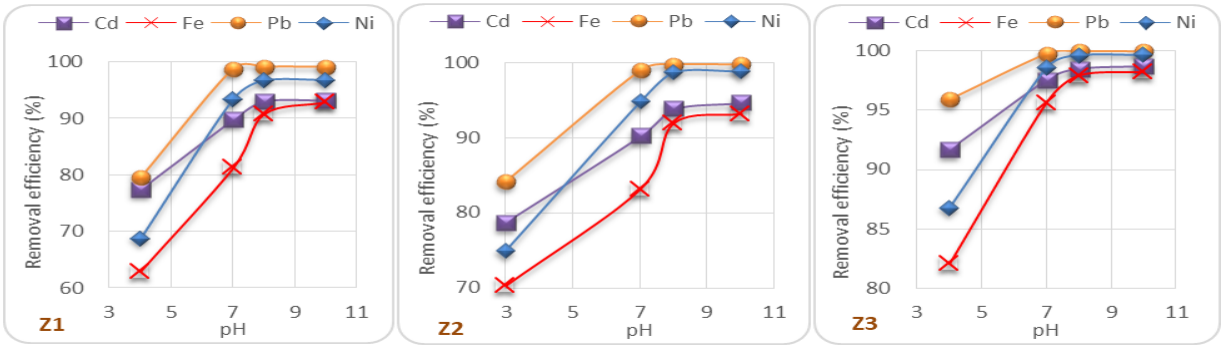

Fig. 13. Effect of pH on adsorption of (Cd(II), Fe(II), Pb(II), and Ni(II)) by zeolite products Z1, Z2, and Z3.

3.4. Regeneration of spent zeolites

The most significant issue in wastewater treatment is the regeneration of spent adsorbent materials [34]. Regeneration is an alternative to disposal for spent zeolites [34]. The regeneration removes the contaminant from the spent zeolites, after repeated reuse of adsorbent for adsorption/desorption cycles (5 trials) in the treatment. The outcomes demonstrated that the removal efficiencies for Z1, Z2. and Z3 were

reduced by average 7%, 5%, and 3% after regeneration, Fig. 14. 1 M KCl could adjust the mineral structure by replacing ions originally present in the mineral zeolites (mono-, divalent cations) with K^+ ions in the desorbing KCl solutions to improve the mineral performance during the recovery cycles. Besides, the increment of metal take-up could be ascribed to the development of complexes among chlorides and metals. Specifically, during the desorption interaction chloride ions could be captured in the cavities of zeolites. The difference in the adsorption between the Z1, Z2, and Z3 could be attributed to the surface area which decreases in the following order Z3<Z2<Z1.

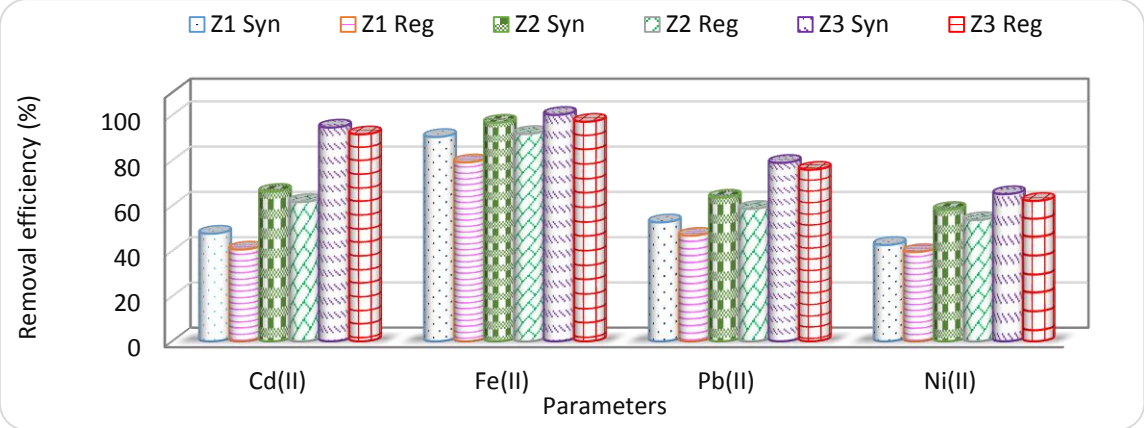

Fig. 14. Percentage of removal efficiency (RE%) Cd(II), Fe(II), Pb(II), and Zn(II) removed from wastewater by synthesized zeolites Z1, Z2, and Z3 before (Syn) and after regeneration (Reg).

4. Conclusion

Different Zeolite structures synthesized via fly ash and sodium hydroxide (NaOH) have good adsorption affinity for Cd(II), Ni(II), Fe(II), and Pb(II) from artificially contaminated water. The conditions of synthesizing zeolite Z1, Z2, and Z3 are fusion reaction conditions of 550 °C for 2 hours, NaOH:FA = 1:1, 1:1.2, and 1:1.4, Si/Al = 2.02, and hydrothermal treatment conditions of 45 °C for 48 h. The outcomes demonstrated that the change in NaOH ratio to fly ash resulted in an effect on the produced phase, crystallite size, and morphology. From the SEM, XRD, and Brunauer-Emmett-Teller (BET) analyses of the zeolite products conducted, the optimum ratio NaOH/CFA for zeolite synthesis is in a specific order 1:4> 1:2 > 1: 1. N_2 adsorption/desorption isotherms demonstrated that the synthetic zeolites were mesoporous and microporous materials with a higher specific area (347, 240, and 127 m^2/g) than the values for raw fly ash ($15m^2/g$). The X-ray diffraction result suggested This research is supported by National Water Research Center, Egypt. The authors are also grateful to the Director of Water Management Research Institute (WMRI), and the Director of Central Laboratory for Environmental Quality Monitoring (CLEQM) for assisting and giving us a chance to complete this study.

that the synthetic products mainly belonged to zeolite phillipsite, carbonate cancrinite, and hydroxysodalite. The optimum condition for removal of Cd(II), Fe(II), Pb(II), and Ni(II) from the water was pH 7, contact time 45 min, and 1 g/L dose of Z1, Z2, and Z3 products. The maximum adsorption capacity for Z1, Z2, and Z3 products was in the range 46-47 mg/g. The adsorbed Cd(II), Fe(II), Pb(II), and Ni(II) ions by zeolites Z1, Z2, and Z3 can be eluted utilizing 1M KCl solution.

Further investigations are needed to identify the efficiency of removal for the physical and chemical properties of wastewater by synthetic zeolites and conduct an on-site pilot-scale study.

5. Acknowledgements

The authors are most appreciative to the working staff for their valuable cooperation.

6. Conflicts of interest

The authors declare no conflict of interest.

7. Reference

1) Ibrahim, L.A., El Gammal, H.A.A., & Mahran, B.N. In vitro, Appraisal and abatement of drainage wastewater pollution in light of utilizing fly ash. *Nat. Sci.* **2017**, 15, 12.
2) Cheng T., Chen C., Tang R., Han C.H., Tian Y. Competitive adsorption of Cu, Ni, Pb, and Cd from aqueous solution onto fly ash-based linde F(K) Zeolite, Iran, *J. Chem. Chem. Eng.* **2018**, 37, 61–72.
3) Prabhu P.P., Prabhu B. A review on removal of heavy metal ions from waste water using natural / modified bentonite, *Int. Con Res. Mech. Eng. Sci. (RiMES 2017), METAC Web Con. EDP Sci*, **2018**, 1–13.
4) Shubaira, T., Eljamala O., Taharab A., Sugiharaa Y., Matsunaga N. Preparation of new magnetic zeolite nanocomposites for removal of strontium from polluted waters. *J Mol. Liq.*, **2019**, 288, 111026.
5) Falyounaa, O., Eljamala, O., Maamouna, I., Taharab, A., Sugiharaa, Y. Magnetic zeolite synthesis for efficient removal of cesium in a lab-scale continuous treatment system. *J. Colloid Interface Sci.* **2020**, 571, 66.
6) Ibrahim, L.A., Chemical characterization and mobility of metal species in fly ash-water system, *Water Sci*, **2015**, 29, 109–122.
7) Wesche, K. Fly ash in concrete: properties and performance, *CRC Press, a Taylor & Francis Book*, London, **2019**.
8) Shah, S.F.A., Aftab, A., Soomro, N., Nawaz, M.S., Vafai, K. Waste Water Treatment-Bed of Coal Fly Ash for Dyes and Pigments Industry, Pak. *J. Anal. Environ. Chem.* **2015**, 16, 48 – 56.
9) Kruger, R.A. Souh African Coal ash Association, *Pers. Comm., Johannesburg*, **2002**.
10) Kutchko B.G. and Kim A.G. Fly ash characterization by SEM-EDS, *Fuel*, **2006**, 85, 2537-2544.
11) Jiangjiang, C., Ouyang, T., Limin, L., Wenzhi, C. Utilization of Coal Fly Ash for Remediation of Metal Contaminated Soil in Mining Sites. *2010 4th Int. Con. Bioinform. Biomed. Eng.*, **2011**, 18-20.
12) Zhang, M., Guo, H., El-Korchi, T., Zhang, G., Tao, M. Experimental feasibility study of geopolymer as the next-generation soil stabilizer. *Constr. Build. Mater*. **2013**, 47, 1468–1478.
13) Nalbantoğlu, Z. Effectiveness of Class C fly ash as an expansive soil stabilizer. *Constr. Build. Mater*. **2014**, 18, 377–381.
14) Güllü, H. Factorial experimental approach for effective dosage rate of stabilizer: application for fine-grained soil treated with bottom ash. *Soils Found.* **2014**, 54, 462–477.
15) Yilmaz, Y. Compaction and strength characteristics of fly ash and fiber amended clayey soil. *Eng. Geol.* **2015**, 188, 168–177.
16) Çiçekm, T., Çinçin, Y. Use of fly ash in production of light-weight building bricks. Constr. *Build. Mater.* **2015**, 94, 521–527.
17) Li, Y, Yang L., Li, X., Miki, T., Nagasaka, T.A composite adsorbent of ZnS nanoclusters grown in zeolite NaA synthesized from fly ash with a high mercury ion removal efficiency in solution, *J. Hazard. Mater.* **2021**, 411, 125044.
18) Nowak, P., Muir, B., Solińska, A., Franus, M., Bajda, T. Synthesis and Characterization of Zeolites Produced from Low-Quality Coal Fly Ash and Wet Flue Gas Desulphurization Wastewater. *Materials*. **2021**, 14(6):1558. https://doi.org/10.3390/ma14061558
19) Iqbal, A., Sattar, H., Haider, R., Munir, S. . Synthesis and characterization of pure phase zeolite 4A from coal fly ash, *J. Clean. Prod.* **2019**, 219, 258–267.
20) Medeiros, F.K.de, Rodrigues, A.M.T., Silva, H.C., Alves, J.B.de B., Ferreira, H.S. Sodalite and cancrinite formation from fly ash: Rietveld and rational chemical analyzes, *Cerâmica*, **2017**, 63, 446-454.
21) Molina, A., Poole, C. A comparative study using two methods to produce zeolites from fly ash, *Mineral. Eng.* **2004**, 17, 167–173.
22) Cundy, C.S., Cox, P.A. The hydrothermal synthesis of zeolites: precursors, intermediates and reaction mechanism. *Micropor Mesopor Mat.* **2005**, 82, 1–78.
23) Visa, M. Synthesis and characterization of new zeolite materials obtained from fly ash for heavy metals removal in advanced wastewater treatment, *Powder Technol.* **2016**, 294, 338–347.
24) Joseph, I.V., Tosheva, L., Doyle, A.M. Simultaneous removal of Cd(II), Co(II), Cu(II), Pb(II), and Zn(II) ions from aqueous solutions via adsorption on FAU-type zeolites prepared from coal fly ash, *J Environ. Chem. Eng.* **2020**, 8, 103895.
25) Tang, H., Xu, X., Wang, B., Lv, C., Sh, D. Removal of Ammonium from Swine Wastewater Using Synthesized Zeolite from Fly Ash, *Sustainability*, **2020**, 12, 3423.
26) Belviso, C., Cavalcante, F., Fiore, S. Synthesis of zeolite from Italian coal fly ash: differences in crystallization temperature using seawater instead

of distilled water. *Waste Manag*. **2010**, 30, 839–847.
27) Yanqing, Y., Xiaoliang, L., Xiaolan, Z., Xiaobin, Z. Effect of seawater salinity on the synthesis of zeolite from coal fly ash. *Front. Environ. Sci. Eng.* **2014**, 8, 54-61.
28) Standard Methods for the Examination of Water and Wastewater; 21st ed.; *American Public Health Association (APHA) Inc.* New York, NY, USA, **2005**.
29) Miller, W.P., Miller, D.M., A Micro-pipette method for soil mechanical analysis. *Comm. Soil Sci. Plant Anal.* **1987**, 18, 1-15.
30) Standard Test Methods for Sampling and Testing Fly Ash or Natural Pozzolans for Use in Portland-Cement Concrete, Designation, *American Society for Testing Materials Standards, © ASTM Int., US*, vol. 04.01 & 04.02, , **2004**.
31) Treacy, M.M.J., Higgins, J.B., Collection of Simulated XRD Powder Patterns for Zeolites, *5th ed, Elsevier, Amsterdam*, 2007.
32) Ibrahim, L.A., ElSayed E.B. Performance Evaluation of Suez Bay Industrial Wastewater Treatment Plant Case Study: Ataqa Region, Egypt. *World J Environ. Biosci.* **2019**, 8,1-11.
33) Ibrahim, L.A., Asaad, A.A., Khalifa, E.A., 2019. Laboratory Approach for Wastewater Treatment Utilizing Chemical Addition Case study: El-Rahway Drain, Egypt. *Life Sci. J.* **2019**, 16, 56-67.
34) ElBastamy, E., Ibrahim, L.A., Ghandour, A., Zelenakova, M., Vranayova, Z., Abu-Hashim, M., Efficiency of Natural Clay Mineral Adsorbent Filtration Systems in Wastewater Treatment for Potential Irrigation Purposes. *Sustainability*. **2021**, 13, 5738.
35) Soil Survey Staff. Soil Taxonomy: A Basic System of Soil Classification for Making and Interpreting Soil Surveys. *U.S. Dept. of Agric. Handb. 436. U.S. Govt.* **1975**.
36) Jha, B., Singh, D.N. A review on synthesis, characterization and industrial application of fly ash zeolites. *J. Mater. Edu*. **2011**, 33, 65–132.
37) Murayama, N., Yamamoto, H., Shibata, J. Mechanism of zeolite synthesis from coal fly ash by alkali hydrothermal reaction, *Inter. J. Miner. Process*. **2002**, 64, 1–17.
38) Sukmak P., Silva P.D., Horpibulsuk, S., Chindaprasirt, P. Sulfate resistance of clay-portland cement and clay high-calcium fly ash geopolymer. *J Mater. Civ. Eng.* **2014**, 27, 04014158.
39) Martens, J.A., Jacobs, P.A., in: J.C. Jansen, M. Sto¨cker, H.G. Karge, J. Weitkamp (eds.). Advanced Zeolite Science and Applications, Studies in Surface Science and Catalysis, *Elsevier*, Amsterdam, vol. 85, 653, **1994**.
40) Tatic, M.,Drzaj, B. Zeolites. B Drzaj, S Hocevar, S Pejvonik (eds), *Elsevier Science Publishers*, Amsterdam, **1985**.
41) Querol, X., Plana, F., Alastuey, A., Lopez-Soler, A. Synthesis of Na-zeolites from fly ash. *Fuel.* **1997**, 76, 793-799.
42) Esaifan, M., Warr, L.N., Grathoff, G., Meyer, T., Schafmeister, M-T., Kruth, A., Testrich, H. Synthesis of Hydroxy-Sodalite/Cancrinite Zeolites from Calcite-Bearing Kaolin for the Removal of Heavy Metal Ions in Aqueous Media. *Minerals*. **2019**, 9, 484. https://doi.org/10.3390/min9080484
43) Reyes, C.A.R.; Williams, C.; Alarcón, O.M.C. Nucleation and growth process of sodalite and cancrinite from kaolinite-rich clay under low-temperature hydrothermal conditions. *Mater. Res*. **2013**, 16, 424.
44) Liu, Y.; Wang, G.; Luo, Q.; Li, X.; Wang, Z. The thermodynamics and kinetics for the removal of copper and nickel ions by the zeolite Y synthesized from fly ash. *Mater. Res. Express*, **2019**, 6.
45) Qiu W., Zheng Y. Removal of lead, copper, nickel, cobalt, and zinc from water by a cancrinite-type zeolite synthesized from fly ash. Chem. Eng. J., **2009**, 145, 483–488.
46) Pandiangan, K.D., Arief, S., Jamarun, N., Simanjuntak, W. Synthesis of zeolite-X from rice husk silica and aluminum metalas acatalyst for transesterification of palm oil, *J. Mater. Environ. Sci.*, **2017**, 8, 1797-1802.
47) Deng, Y, Flury, M., Harsh, J.B., Felmy, A.R., Qafoku, O. Cancrinite and sodalite formation in the presence of cesium, potassium, magnesium, calcium and strontium in Hanford tank waste stimulants. *J. Appl. Geochem.* **2006**, 21, 2049-2063.
48) Golomeova, M., Zendelska, A., Blažev, K., Krstev, B., Golomeov, B. Removal of heavy metals from aqueous solution using clinoptiloliteand stilbite. *Int. J. Eng. Res. Technol.* **2014**, 3, 1029–1035.
49) Aljerf, L., High-efficiency extraction of bromocresol purple dye and heavy metals as chromium from industrial effluent by adsorption onto a modified surface of zeolite: kinetics and equilibrium study, J. *Environ. Manag.* **2018**, 225, 120–132.